Journal of Controlled Release 295 (2019) 21–30

Contents lists available at ScienceDirect

Journal of Controlled Release

journal homepage: www.elsevier.com/locate/jconrel

Microfluidic assembly of hydrogel-based immunogenic tumor spheroids for evaluation of anticancer therapies and biomarker release

Pooja Sabhachandani[a,1], Saheli Sarkar[a,1], Seamus Mckenney[a], Dashnamoorthy Ravi[b], Andrew M. Evens[b], Tania Konry[a,*]

[a] Department of Pharmaceutical Sciences, Northeastern University, 360 Huntington Avenue, Boston, MA 02115, USA
[b] Division of Blood Disorders, Rutgers Cancer Institute of New Jersey, New Brunswick, NJ

ARTICLE INFO

Keywords:
3D culture
Alginate
Immunogenic spheroid
Microfluidics
Puramatrix

ABSTRACT

Diffuse large B cell lymphoma (DLBCL), the most common subtype of Non-Hodgkin lymphoma, exhibits pathologic heterogeneity and a dynamic immunogenic tumor microenvironment (TME). However, the lack of preclinical in vitro models of DLBCL TME hinders optimal therapeutic screening. This study describes the development of an integrated droplet microfluidics-based platform for high-throughput generation of immunogenic DLBCL spheroids. The spheroids consist of three cell types (cancer, fibroblast and lymphocytes) in a novel hydrogel combination of alginate and puramatrix, which promoted cell adhesion and aggregation. This system facilitates dynamic analysis of cellular interaction, proliferation and therapeutic efficacy via spatiotemporal monitoring and secretome profiling. The immunomodulatory drug lenalidomide had direct anti-proliferative effect on activated B-cell like DLBCL spheroids and reduced several cytokines and other markers (e.g., CCL2, CCL3, CCL4, CD137 and ANG-1 levels) compared with untreated spheroids. Collectively, this novel spheroid platform will enable high-throughput anti-cancer therapeutic screening in a semi-automated manner.

1. Introduction

Diffuse large B- cell lymphoma (DLBCL) is the most common subtype of non-Hodgkin lymphoma (NHL), accounting for > 30% of all NHLs diagnosed each year in the United States [1]. The survival and progression of DLBCL in lymphoid tissues has been shown to be regulated by the interaction of malignant B cells with stromal fibroblasts, endothelial cells and various types of immune cells including dendritic cells (DC), T cells and natural killer cells [2–4]. The dynamic crosstalk with stromal cells provide pro-survival cues to DLBCL cells, which may lead to therapeutic failure and the emergence of drug resistant tumor phenotypes [5,6]. A novel strategy in DLBCL treatment aims to target the microenvironment in part to minimize DLBCL cell signaling and crosstalk with stromal components. However, there are few experimental models currently available to optimally test dynamic cellular interaction, survival and response of DLBCL cells to chemotherapy and immunotherapeutic drugs in a highly heterogeneous microenvironment. Some studies have utilized immunocompromised or syngeneic murine models, where tumor cell lines are implanted at nodal or extranodal locations [7]. The tumor response in such models is dependent on the site of implantation. Furthermore, the high cost and labor involved with animal models preclude concurrent testing of multiple drugs and drug combinations [8]. Thus, it is essential to develop high throughput in vitro models of lymphoma that permit effective monitoring of the tumor microenvironment (TME) and interaction between cancer, immune and non-immune stroma during therapeutic screening.

Current in vitro methods used for the evaluation of therapeutic efficiency are predominantly two dimensional (2D) [9–11]. 2D cultures do not mimic growth profiles and cellular organization observed in vivo and often lack the heterogeneity of TME [12]. In contrast, three-dimensional (3D) models recreate cell shape, polarization and spatial constraints observed in physiological environments and also provide information on the biophysics of cell-extracellular matrix (ECM) interactions. 3D models have been broadly classified into transwell-type, spheroids, combination and microvasculature-based systems [13]. Spheroids are widely used for characterizing cancer cell responses; however, existing techniques for generation of spheroids, such as hanging drops or non-adherent well plates, have numerous limitations including low throughput and inefficient long-term culture [13]. To date, few studies have reported the use of 3D tumor spheroids for

* Corresponding author.
E-mail address: t.konry@northeastern.edu (T. Konry).
[1] These authors contributed equally to this work.

https://doi.org/10.1016/j.jconrel.2018.12.010
Received 6 September 2018; Received in revised form 3 December 2018; Accepted 7 December 2018
Available online 12 December 2018

monitoring therapeutic efficiency in vitro in DLBCL [14]. These spheroids, called "multicellular aggregates of lymphoma cells", were generated by the hanging drop method with lymphoma cells alone. The study did not assess lymphoma-immune cell interaction or cell-ECM interaction in spheroids. These factors have a strong impact on DLBCL progression as well as response to drug treatment. Therefore, it is necessary to address the drawbacks of the conventional systems and develop a high throughput method for generation of 3D immunogenic tissue-like constructs that simulate heterogeneous TME. Such a platform could facilitate analysis of cell survival, interaction and efficacy of anti-tumor therapeutics [15].

Microfluidic methods have been employed previously to form tumor spheroids by cell aggregation [16,17]. Advances in 3D printing have promoted the fabrication of several bioprinted organ-on-a-chip systems as well as cancer spheroids [18]. While most reports focus on multicellular spheroids, omitting cell-ECM interaction, Jeong et al. cultured cancer and fibroblasts in a collagen-incorporated microfluidic chip [19]. Our group has also developed 3D breast cancer co-culture spheroids in a droplet microfluidic platform [20]. The microfluidic spheroids were maintained long-term (14 days) on-chip via a perfusion system and used for functional assessment of chemotherapeutic drug resistance. But none of these studies included an immunogenic component in the spheroids to allow monitoring of cancer-immune cross-talk. Recently, a few reports assessed various aspects of cancer responses such as migration, extravasation and ex vivo propagation in the presence of immune cells in different types of microfluidic channels [20–22]. The channels were filled with Type I collagen to provide a barrier for modeling intravasation in the presence of macrophages [21]. Another study determined the motility of conditioned DCs towards colorectal cancer cells treated with epigenetic drugs and interferon α in collagen-embedded microchannels [22]. However, the microchannel format is not suitable for generation of individual spheroids containing both cells and matrices, thereby limiting experimental throughput. Also, none of the studies investigated lymphoma cell interactions, either in microfluidic channels or spheroids. The spheroid model is more representative of NHL, which grows as spherical tumors.

This study describes the development of a novel droplet microfluidics- based approach for generation of 3D tumor-stromal-immune cell spheroids using composite hydrogel for on-chip assessment of immunomodulatory drug activity. Our study utilizes an integrated high-throughput microfluidic droplet docking array which traps the spheroids on-chip to evaluate dynamic cell response to immunotherapy. The spheroids are continually perfused with drugs, and the cell secretions are collected at routine intervals for proteomic analysis. The heterogeneous TME of NHL was recreated by incorporating three cell types in the spheroids- lymphoma, fibroblasts and peripheral blood mononuclear cells (PBMC), which have not been reported previously. The hydrogel base of the constructs was composed of alginate and puramatrix, a synthetic peptide with a fiber network resembling the structure of naturally occurring ECM gels [23,25,26]. Our results suggest that the composite hydrogel increased cell aggregation and proliferation compared with alginate alone. We verified the applicability of the microfluidic spheroids in immunomodulatory drug screening by determining the anti-cancer effect of lenalidomide [27]. Our results demonstrate that lenalidomide enhanced overall death of cancer cells in the presence of activated immune cells and downregulated a number of pro-inflammatory cytokines, further contributing to anti-tumor effect in the TME. The developed microfluidic spheroid platform can thus be used for multiparametric analysis of drug susceptibility and high-throughput immunotherapeutic screening.

2. Materials and methods

2.1. Microfluidic device design and fabrication

Preparation of the microfluidic devices using soft lithography was conducted as discussed previously [20]. Negative photo resist SU-8 2100 (MicroChem, Newton, MA) was patterned on the silicon wafers to a thickness of 150 μm. This was then exposed to UV light through a transparent photomask (CAD/Art Services, Bandon, OR). Polydimethylsiloxane (PDMS) (Sylgard 184, Dow Corning, Midland, MI) and its crosslinker were mixed at a ratio of 10:1 and poured onto the device template generated on the silicon wafers. This was subsequently degassed and cured for 12 h at a temperature of 65 °C. The cured PDMS with the etched microfluidic cannels was then peeled off from the wafers, cut into individual devices and bonded to glass slides after oxygen-plasma treatment of both surfaces. To make the microfluidic channels hydrophobic for efficient droplet generation, devices were treated with Aquapel (PPG Industries, Pittsburg, PA) for 20 min prior to the experiment. Subsequently the Aquapel was expelled by flushing the device with air. All the liquids for droplet generation (cell solutions, oil, etc.) were introduced into the device using Tygon Micro Bore PVC Tubing (dimensions: 0.010″ ID, 0.030″ OD, 0.010″ wall) (Small Parts Inc., FL, USA). Sterile, disposable 1 mL syringes were utilized to load the oil, cell and polymer solutions onto the devices connected by the tubing. The input of the solutions was regulated by syringe pumps (Harvard Apparatus, USA) to control flow rates. The oil phase used for droplet generation consisted of mineral oil and 2% (*w/v*) of surfactant Span80 (Sigma-Aldrich, St. Louis, MO).

2.2. Rheological characterization of alginate-puramatrix hydrogel

Hydrogel solutions containing 1% w/v alginate and 0–0.25% *v*/v puramatrix were prepared and kept at 4 °C. The viscoelastic properties of the hydrogels were analyzed using a Discovery HR1 hybrid rheometer (TA Instruments, Newcastle, DE) equipped with a with temperature control unit (Peltier plate, ± 0.05 °C) operated in the cone-plate mode with a cone angle of 1° and a 40 mm diameter. Storage (G') and loss (G") moduli were measured for solutions of 1% alginate, 1% alginate/0.15% puramatrix and 1% alginate/0.25% puramatrix in a frequency range of 0.1–10 Hz at 25 °c, while viscosity was measured at 25 °C and 37 °C, after initial equilibration at 4 °C, at a frequency of 1 Hz.

2.3. Scanning electron microscopy

Alginate-puramatrix (1% alginate, 0.15% puramatrix) spheroids were seeded with SUDHL-10 cells at a concentration of 3×10^6 cells mL^{-1}. After incubation for 1–6 days at 37 °C and 5% CO_2 in RPMI media, the spheroids were fixed in 2.5% gluataraldehyde, 2.5% (para) formaldehyde in 0.1 M sodium cacodylate (pH 7.2) for 1 h at 25 °C. The samples were washed with 0.1 M sodium cacodylate buffer (pH 7.2) and dehydrated through a graded ethanol series (30%, 50%, 70%, 85%, 95%, 100%) for 10 min each. The spheroids were subjected to critical point drying with liquid CO_2 using a Samdri-PVT-3D critical point dryer (Tousimis, Rockville MD) to complete the drying process. Dried samples were adhered onto an aluminum mount with carbon adhesive tabs and coated with 6 nm of platinum using a 208HR sputter coater equipped with a MTM-20 thickness controller (Cressington, Watford, England). SEM images were captured with a Hitachi S-4800 field emission scanning electron microscope (Hitachi, Japan) at an accelerating voltage of 2–3 kV.

2.4. Cell culture

SUDHL-10 cells (DLBCL line) and HS-5 cells (fibroblast line) were originally purchased from American Type Culture Collection (ATCC, Manassas, VA). The SUDHL-10 cells were maintained in RPMI 1640 media supplemented with 10% fetal bovine serum and 1% antibiotic-antimycotic solution (Corning Cellgro, Manassas, VA) and the HS-5 cells were maintained in DMEM medium with 4.5 g L^{-1} glucose and L-glutamine (Corning Cellgro, Manassas, VA) with serum and antibiotic-antimycotic solution.

Peripheral Blood mononuclear cells (PBMCs) were obtained from Astarte bio (Astarte Biologics, Bothell, WA) and subsequently treated to generate activated PBMCs. Briefly, anti-CD3 antibody was used to coat well plates at a concentration of 10 μg mL^{-1} for a period of 2 h. The cells were then seeded at a concentration of 15, 000 cells per well along with an activation cocktail consisting of IL-2 (10 ng mL^{-1}), IL-4 (20 ng mL^{-1}) and soluble anti-human CD-28 antibody (2 μg mL^{-1}) for two days. The plate was centrifuged and re-treated for another two days with IL-2 (10 ng mL^{-1}) and IL-4 (20 ng mL^{-1}). The cells were then harvested, washed and resuspended in fresh IL-2 containing media for experiments.

All cells were grown at 37 °C under 5% CO_2 in a humidified atmosphere. Cells were routinely passaged every three days and harvested at a density of 1×10^6 viable cells mL^{-1}.

2.5. Spheroid generation and maintenance in microfluidic device

Sodium alginate (Sigma) was dissolved in media at a concentration of 1% *w/v* by constant agitation at 50 °C for 2 h. The solution was stored at 4 °C for a maximum of 2 weeks. Puramatrix (BD Biosciences, Franklin Lakes, NJ) is provided as a 1% *w/v* solution by the manufacturer and was stored at 4 °C prior to use. It was diluted into various concentrations in the previously prepared alginate solution (0.05%–0.25% *v/v*) immediately prior to use and was maintained at 4 °C. Calcium chloride (2% w/v, Sigma) solution was prepared in media and sterile filtered using a 0.22 μm syringe filter. It was stored at 4 °C for a maximum of 2 weeks.

Spheroid generation in the microfluidic device was a multi-step process as follows: the first step was the generation the polymer droplets containing the cell suspension and the second step was the gelation of the droplets in the docking array by the calcium chloride solution (2% *w/v* ≈ 175 mM). 10×10^6 cells mL^{-1} were used for spheroid generation and for co-culture experiments the cells were used at a ratio of 3:1 (PBMC: tumor and stroma). The cells were suspended in the polymer solution and introduced into the microfluidic device at a flow rate of 75 μL h^{-1} and oil was flown at 500 μL h^{-1} through the oil inlet. Once the docking array was filled with cell laden droplets, calcium chloride solution was allowed to flow through the third inlet at the rate of 1 μL h^{-1} for 4–5 h for the gelation to occur. Once gelled, the spheroids were stable in the docking array for extended periods of time. Complete media and/or drug solution was perfused through the spheroids in the array for the experimental period (5 days) at a flow rate of 50 μL h^{-1}. For lenalidomide experiments, the spheroids were treated with a therapeutically relevant concentration of 2.3 μM for a period of 5 days by continuous perfusion. All images were obtained using Zeiss Axio Observer. Z1 Microscope (Zeiss, Germany) equipped with Hamamatsu digital camera C10600 Orca-R2.

2.6. Proliferation and cytotoxicity assessment

Cell proliferation was determined by labeling the cells in the spheroids fluorescently with different cell proliferation trackers (Life Technologies, Carlsbad, CA). SUDHL-10, HS-5 and PBMCs (activated and non-activated) cells were labeled with CFSE cell proliferation dye (ex/em: 492/517 nm) for single cell type spheroid experiments. For co-culture spheroid experiments, activated and non-activated PBMCs were labeled with CFSE dye and the SUDHL-10 and HS-5 cells were labeled with CMAC cell proliferation dye (ex/em: 353/466 nm). For specific experiments, PBMCs were labeled with CMAC, SUDHL10 cells were labeled with CFSE and HS5 cells were labeled with CMTPX cell proliferation dye (ex/em: 577/602). Cell death was indicated by the uptake of ethidium homodimer-1 (EthD-1) (ex/em: 495/635 nm) at the end of day 5.

Cells were counted on day 1 and day 5; the increase in cell number was normalized to initial (day 1) cell counts and reported as percent proliferation. For cell death analysis, the cells with red fluorescence of EthD-1 were counted at day 5 and percent death was calculated by dividing the number of dead cells by total number of cells at day 5.

2.7. Cell response in 2D monolayers

Viability in immunogenic microfluidic spheroids was compared with viability in 2D monolayer cultures. Cells were seeded at a density of 7500 cells per well and treated with lenalidomide as in the microfluidic experiments (2.3 μM for 5 days).

2.8. Secretion analysis

The media perfused through the microfluidic spheroids for all treatment conditions was collected at 24 h intervals for 5 days. These perfusions were analyzed for 92 protein biomarkers using Proseek Multiplex® immune-oncology panel (Olink Proteomics, Uppsala, Sweden). Processing, output data quality check, and normalization were performed by Olink Proteomics. All values were presented as Normalized Protein expression (NPX) values on a log2 scale. The log2 NPX values were scaled to mean 1 and SD 1 before data analysis, to facilitate comparisons between protein associations. Data values below the level of detection (LOD) are highlighted in red.

2.9. Statistical analysis

The cell numbers were measured using the colony counting extension of ImageJ software (https://imagej.nih.gov/). For all studies with microfluidic spheroids, a minimum of 30 spheroids was analyzed for every condition, and $n = 2$ experimental repeats were conducted [20]. For 2D monolayer culture, all conditions were repeated in triplicates. Statistical analysis was done by comparing the data sets using the student's *t*-test, and p value < 0.05 was considered statistically significant.

3. Results

3.1. Rheological characterization of alginate and puramatrix combination polymer for spheroid generation

Alginate has been used previously in combination with collagen, fibrin and matrigel to promote cell survival and growth in tumor spheroids [28–30]. However, alginate does not express cell-binding moieties, which makes it challenging to observe cell proliferation and subsequent interaction in alginate gels. In this study, we combined alginate with puramatrix to increase cell adhesion and aggregation. Puramatrix has low pH (pH = 3 at 1% solution), which could potentially reduce cell viability [23]. To minimize this effect, puramatrix was diluted (0.1–0.25%) and added to 1% *w/v* alginate in the combination hydrogels.

Extensive rheological characterization of the mixed hydrogel combinations was performed prior to microfluidic application (Fig. 1). Since the hydrogel solution must be continuously flown in the microfluidic platform to generate droplets, it is necessary to assess the viscosity of the hydrogel prior to gelation so as to ensure smooth flow of cell and aqueous gel streams. Here, dynamic viscosity of the alginate-puramatrix hydrogel, defined as the measure of the fluid's internal resistance to flow, was measured. The viscosity of the combination hydrogel, prepared by mixing a range of puramatrix (0.05–0.25%) dilutions with 1% *w/v* alginate, was compared to non-modified 1% alginate solution at 25 °C and 37 °C (Fig. 1A). Dynamic viscosity did not vary significantly for puramatrix concentrations up to 0.10% (0.01 ± 0.005 Pa. S) but increased thereafter with increase in puramatrix concentration (0.20–0.25%). Next, the storage modulus (G'), indicating elastic behavior, and the loss modulus (G"), indicating viscous response was determined at frequencies 0.1–10 Hz. As shown in Fig. 1B, G" of alginate is greater than G', particularly at lower frequencies (0.1-1 Hz), depicting liquid-like responses. The addition of puramatrix reversed the response

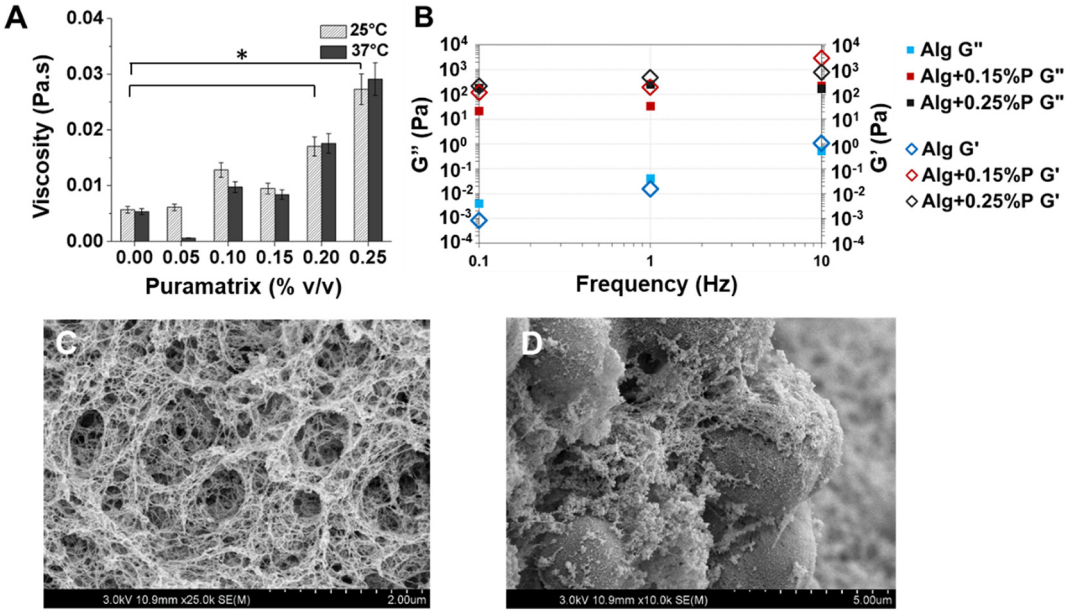

Fig. 1. Rheological characterization of the alginate-puramatrix hydrogel combination. (A) Dynamic viscosity of 1% *w/v* alginate with varying compositions of Puramatrix at 25 °0C and 37 °0C. * indicates $p < 0.05$. (B) Storage modulus (G') and loss modulus (G") for 1% w/v alginate (Alg) with puramatrix (P: 0, 0.15% and 0.25% *v/v*). (C-D) SEM images of 1% w/v alginate with 0.15% v/v puramatrix combination; (C) without cells and (D) with cells. Scale bars: 2 and 5 μm respectively.

(G' > G"), yielding the characteristic behavior of hydrogels. This result suggests that puramatrix increases the elasticity of the combination polymer solution and promotes formation of hydrogels. Lastly, the porosity of the hydrogels was also assessed. The pore size of 0.15% puramatrix-1% alginate combination, which supported cell clustering and proliferation, was found to be 0.005–0.2 μm, while that of 1% alginate was 0.005–0.1 μm (Fig. 1C–D). We also determined cell proliferation in combination hydrogels. Cells aggregated and proliferated in clusters in 0.1–0.25% composite hydrogel, in agreement with previous studies with puramatrix only (Fig. S1) [23]. Based on these data, we selected the combination of 1% alginate and 0.15% puramatrix to form microfluidic spheroids with improved hydrogel strength while maintaining the elasticity offered by puramatrix.

3.2. Fabrication of immunogenic tumor spheroids using droplet microfluidic platform

Here we describe a droplet microfluidics approach for the generation of hydrogel-based 3D lymphoma spheroids (Fig. 2A–B). The microfluidic device can potentially house and monitor 250 cell-laden spheroids in the integrated docking array (Fig. 2A). The generation of spheroids occurred in two stages. In the first stage, droplets containing cells and liquid hydrogel (1% alginate and 0.15% puramatrix) were formed at the T-junction and driven into the docking array (Fig. 2C–D). The individual docking sites for the spheroids are 400 μm in diameter. The optimal droplet size was thus maintained at 350 ± 25 μm in diameter to prevent neighboring droplets in the array from merging prior to gelation. The second phase occurs after stabilizing the droplets in the docking array. Calcium chloride (2% *w/v* solution) in complete growth media was perfused at a slow and controlled rate of 2 μL/h to ionically crosslink the hydrogel in droplets (Fig. 2E) [20]. This external gelation mechanism allows for polymerization of the hydrogels in situ while the slow perfusion helps maintain the spherical structure of these constructs.

The solid-phase spheroids are trapped in the docking array for extended periods of time (Fig. 2F), which permitted us to monitor spatiotemporal dynamics in the same spheroid throughout the experimental duration. The generated spheroids were continuously perfused with media/or drug solution at 50 μL/h, equivalent to 575 μm/s, for 5 days. This flow rate mimics the blood velocity in the tumor, which has been reported to vary over a range of 100–800 μm/s, depending on the tumor size in vivo [31]. Continuous perfusion has two advantages in our system: supplying nutrients to the spheroids for cell survival over long periods, and ability to assess cell secretions at specific intervals. Media was collected from the spheroid array outlet every 24 h to quantify cell-secreted factors such as cytokines and chemokines as described below.

The cellular components of the spheroid were selected to mimic the TME of NHL, which is comprised of tumor cells, fibroblasts and immune cells [32,33]. For the tumor cell component, a germinal center B cell (GCB) lymphoma line SUDHL-10 was utilized. The stromal component was represented by bone marrow fibroblast line HS-5 [34]. SUDHL10 and HS-5 cells were mixed at a ratio of 1:1 [19]. Primary peripheral blood mononuclear cells (PBMCs) from healthy donors were incorporated as the immune component. Since 75% of the cell population in the lymphoma TME are immune cells, the initial seeding density ratio of immune cells: non-immune cells (i.e., cancer cells and fibroblast) was maintained at 3:1 (Fig. S2A). Prior to generating a complex co-culture spheroid, control spheroid models consisting of one cell type (SUDHL-10 cells (Fig. S2B), HS-5 cells (Fig. S2C), activated PBMCs (Fig. S2D), and non-activated PBMCs (Fig. S2E) were also formed to test the compatibility of each cell type and the viability in the microfluidic system.

3.3. Effect of immunomodulatory drug on cell survival in tumor spheroids

Several reports have suggested distinct differences in cell survival in 2D monolayers compared to 3D spheroids [19,35]. Here we compared cell survival in 2D monolayer and microfluidic spheroids (Fig. S3, Figs. 3–6). We used two methods to assess overall cell heath in all models: (a) cell proliferation, and (b) overall death at day 5. Given the complex mixture of cells in the immunogenic tumor spheroids, we first determined the viability of cells in monoculture spheroids (i.e., containing one cell type) before progressing to the co-culture models. We further determined the impact of the immunomodulatory drug lenalidomide on cell death, as this drug has demonstrated anti-cancer effects in various types of cancers including lymphoma [34,36,37]. The concentration of lenalidomide tested was 2.3 μM, a relevant concentration

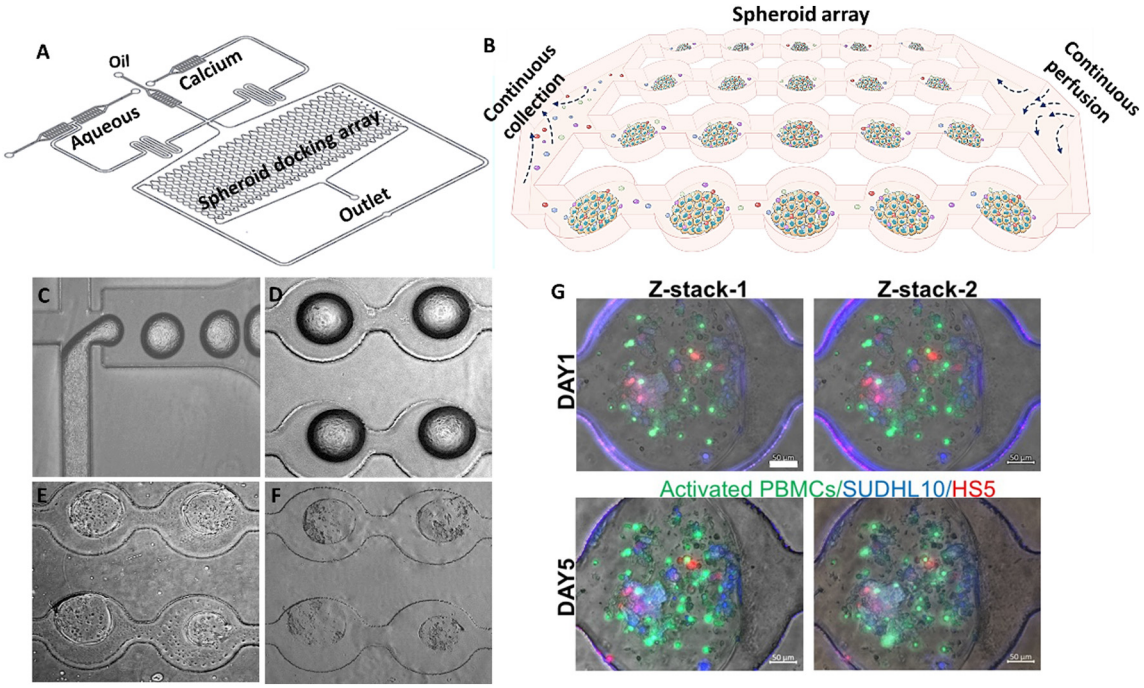

Fig. 2. Development of microfluidic spheroids. (A) Schematics of microfluidic device indicating various inlets. (B) Illustration of the sphere based microarray system. (C) Cell-containing hydrogel droplet generation at the T-junction. (D) Droplet localization in docking array. (*E*-F) Images of gelled spheroids obtained at day 1 (E) and day 5 (F). (G) Tracking cell proliferation in a single 3D construct in the microfluidic device over 5 days. Scale bar: 50 μm.

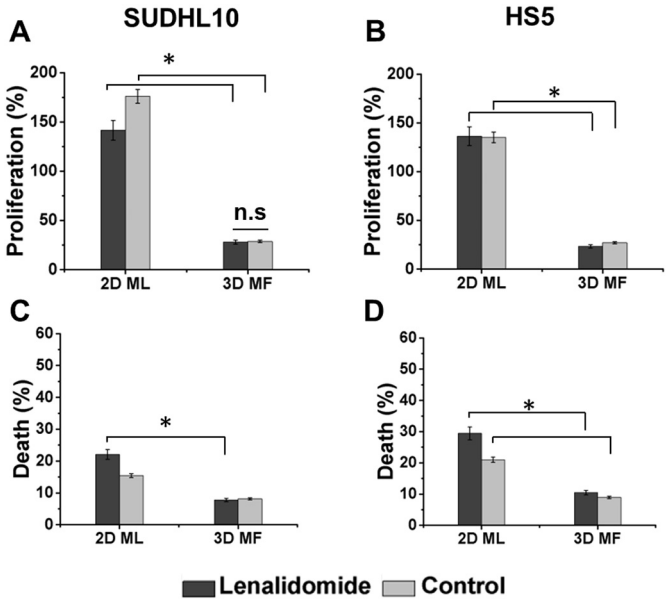

Fig. 3. Cell viability in tumor and fibroblast spheroids. (A-B) Proliferation of SUDHL-10 (A) and HS-5 (B) in 2D monolayer (2D ML) and microfluidic spheroids (3D MF). (C-D) Cell death (%) of SUDHL-10 (C) and HS-5 (D) in monolayer and spheroids. Data obtained from $n = 3$ repeats for monolayer and $n = 2$ for microfluidics. Values indicate mean ± SD. * indicates $p < 0.05$; n.s: non-significant.

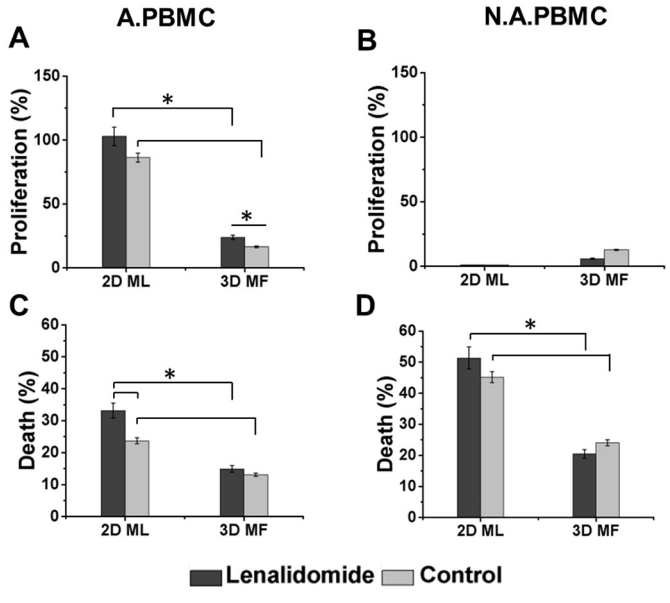

Fig. 4. Cell viability in immune cell spheroids. (A-B) Proliferation of activated PBMC (A.PBMC) (A) and non-activated PBMC (N.A. PBMC) (B) in 2D monolayer (2D ML) and microfluidic (3D MF) spheroids. (C-D) Cell death (%) of A.PBMC (C) and N.A. PBMC (D) in 2D monolayer and MF spheroids. Data obtained from $n = 3$ repeats for monolayer and $n = 2$ for microfluidics. Values indicate mean ± SD. * indicates $p < 0.05$.

used for clinical studies [38].

3.3.1. Viability of tumor-stromal component

Fig. 3 compares the proliferation and survival characteristics of SUDHL-10 and HS-5 cells. SUDHL-10 cells proliferated under control conditions (175% in 2D, 28% in 3D), i.e., in the absence of lenalidomide (Fig. 3A). Conversely, untreated SUDHL10 cell death was limited in all platforms (15% in 2D monolayer vs 8% in 3D microfluidic). However, for the drug treatment condition, the percent death in the 2D monolayer was significantly higher as compared with 3D microfluidic (22% and 7% respectively) (Fig. 3C).

A similar trend of cell proliferation (Fig. 3B) and death (Fig. 3D) was observed in HS-5 fibroblasts, where the cell proliferation was not affected by lenalidomide. Cell death in the 2D monolayer was significantly higher than in 3D spheroids with and without drug treatment (29% vs 10% with drug treatment and 21% vs 8% without drug

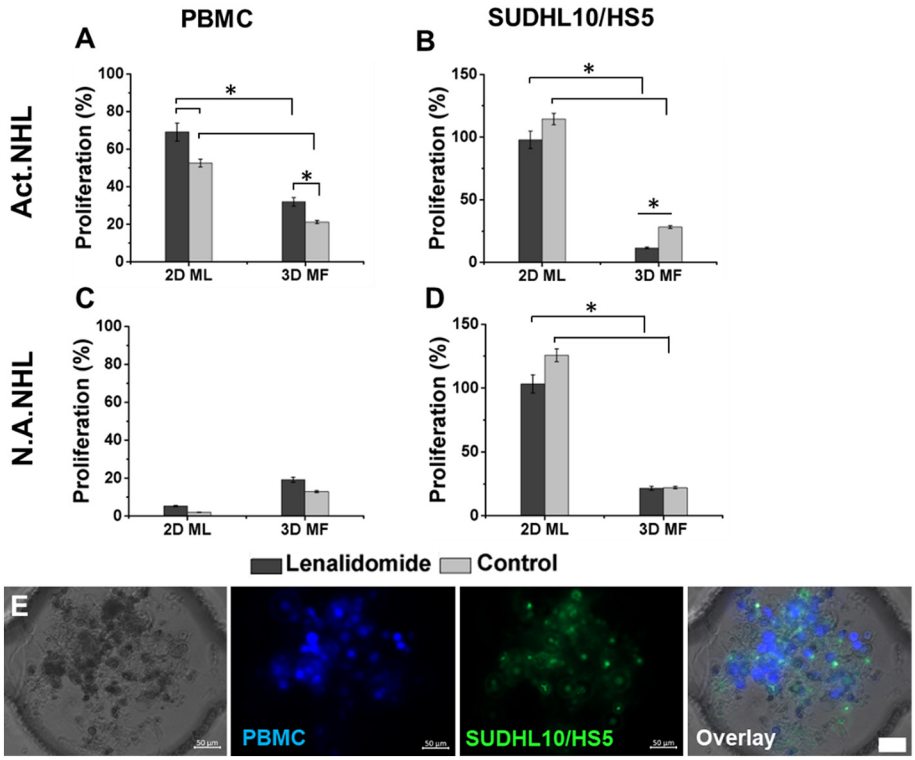

Fig. 5. Cell viability in heterotypic immunogenic NHL spheroids. Activated NHL (Act.NHL) spheroids (A,B) consisted of SUDHL10, HS5 and IL2/IL4/CD28 - activated PBMCs. Non activated NHL (N.A.NHL) spheroids (C,D) consisted of SUDHL10, HS5 and non-activated PBMCs. (A,C) Proliferation of PBMCs in the two types of spheroids. (B,D) Proliferation of non-immunogenic cell types (SUDHL10 and HS5 combined). Cultures were treated with lenalidomide or left untreated (Conrol). Data obtained from $n = 3$ independent repeats for monolayers (2D ML); $n = 2$ for microfluidics (3D MF). Values indicate mean ± SD. * indicates $p < 0.05$. (E) Image of microfluidic spheroid generated with PBMC, SUDHl10 and HS5 cells. Scale bar: 50 µm.

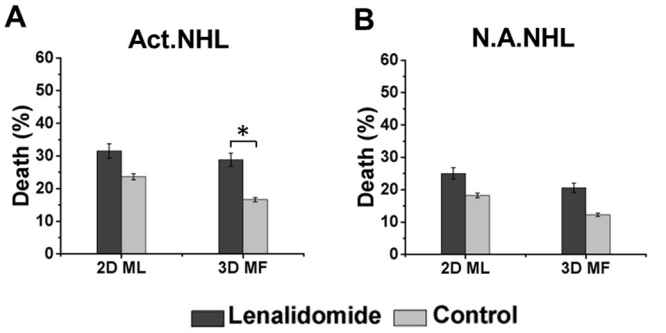

Fig. 6. Quantification of cell death in 2D and 3D immunogenic NHL cell mixtures. Overall death (%) in (A) activated PBMC + SUDHL-10 + HS-5 and (B) non-activated-PBMC + SUDHL-10 + HS-5 cell mixtures. Data obtained from $n = 3$ repeats for monolayer (ML) and $n = 2$ for microfluidics (MF) experiments. Values indicate mean ± SD. * indicates $p < 0.05$.

treatment). Although lenalidomide is not directly cytotoxic against SUDHL-10 and HS-5 cells, it causes a decrease in proliferation in SUDHL-10 monolayer cultures and increase in cell death in SUDHL-10 and HS-5 cells in 2D monolayer compared with the 3D microfluidic format. It is feasible that culturing cells in 2D monolayer makes them more susceptible to cytotoxic action of compounds. Overall, these data showed that 3D hydrogel-based microfluidic spheroids supported SUDHL10 and HS5 proliferation and resulted in decreased cell death in the presence or absence of lenalidomide treatment.

3.3.2. Viability of immune component in spheroids

Lenalidomide suppresses GCB lymphoma cell response indirectly via activated immune cells. Here we compared viability of activated and non-activated PBMCs in microfluidic spheroids with cells in monolayers (Fig. 4). Activated PBMCs proliferated significantly ($p < 0.001$) compared to non-activated PBMCs in both experimental platforms (Fig. 4A-B). Also, lenalidomide increased proliferation of activated PBMCs compared to control (i.e., in the absence of the drug) in all conditions (Fig. 4A). There was no increase in proliferation for non-activated PBMCs for either control or drug treatment conditions (Fig. 4B).

We next measured overall death of PBMCs. As shown in Figs. 4C-D, 3D microfluidic spheroids depicted significantly decreased death for both activated and non-activated PBMCs compared to 2D cultures ($p < 0.05$). As with the other cell lines, 2D monolayer showed increased death for both types of PBMCs (≥25% with and without lenalidomide). These findings demonstrate that PBMC viability was not adversely affected in our microfluidic spheroids as compared to standard culture techniques.

3.3.3. Cell survival in immunogenic tumor spheroids

Immunogenic NHL spheroids were generated using all three cell types i.e., SUDHL-10, HS-5 and activated PBMCs (referred to as ACT-NHL) (Fig. 2G, Fig. 5E). Control spheroids were formed with SUDHL-10, HS-5 and non-activated PBMCs (NA-NHL spheroids) to assess tertiary, non-specific effects of lenalidomide on the viability of the encapsulated cells.

Lenalidomide treatment decreased proliferation of the non-immune (lymphoma and fibroblast) cell types in activated microfluidic spheroids significantly (ACT-NHL, 28% to 11%) ($p < .05$) but not in the non-activated (NA-NHL, 23% to 21%) microfluidic spheroids (Fig. 5B, D) compared to untreated control. Lenalidomide also decreased tumor-stroma proliferation in 2D monolayer for ACT-NHL and NA-NHL (Fig. 5B, D). We further determined the proliferation of specific non-immune cell types (SUDHL10 and HS5) in the co-culture microfluidic spheroids (Fig. S4). While HS5 cell proliferation was not altered by lenalidomide treatment (22% control vs 20.5% lenalidomide), SUDHL10 were downregulated (29% vs 23% in treated and untreated spheroids respectively). This suggested that the reduction in proliferation observed in the immunogenic microfluidic spheroids was due to a decrease in cancer cell proliferation specifically. We then compared the growth of individual cell types in the immunogenic co-culture spheroids (Fig. S4) with mono-culture spheroids (Fig. 3A–B). Proliferation of SUDHL-10, HS-5 and activated PBMCs were comparable in control co-culture spheroids compared to mono-culture spheroids (Table S1).

In assessing the effect of lenalidomide treatment on immune cells,

we observed an increase (52% in untreated vs 70% in treated conditions) ($p < 0.05$) in activated PBMC proliferation in the 2D monolayer (Fig. 5A), which maintained the trend observed in the same experimental approach in mono-culture immune cells (Fig. 4A). A similar increase was observed in 3D microfluidic spheroids (Fig. 5A). Proliferation was limited in 3D spheroids as compared with monolayer, as observed in all cell types. For NA-NHL spheroids, the increase in PBMC proliferation was extremely low in 3D microfluidic spheroids (Fig. 5C); there was no proliferation observed in the 2D monolayer format for the non-activated PBMCs.

We further investigated the overall death in the co-culture model in each platform in the presence and absence of the drug. Cell death was increased from 17% to 29% ($p < 0.05$) in 3D ACT-NHL microfluidic spheroids, as well as in monolayers, due to lenalidomide (Fig. 6A). Similar trends were observed across experimental platforms in the case of NA-NHL (Fig. 6B). However, lenalidomide did not increase death significantly in this case, presumably due to its inability to harness non-activated immune cells [39]. These findings suggest that lenalidomide diminishes growth of cancer cells without actively increasing cell death in microfluidic spheroids. Moreover, the microfluidic platform consistently depicted reduced cell death compared to conventional cell culture platforms.

3.4. Proteomic profile of factors released from 3D microfluidic spheroids

Release of secretory factors such as cytokines and chemokines by the immune cells in the TME plays an important role in tumor progression and response to therapies. Lenalidomide promotes tumor regression by downregulating proinflammatory cytokines, increasing recruitment and activating effector cells (cytotoxic T cells and NK cells) [36]. Since the microfluidic array was continuously perfused with media, we were able to collect conditioned media periodically (every 24 h) from the spheroid array. We investigated a total of ninety two protein biomarkers relevant to various biological processes as shown in Fig. 7. Here, we discuss the ten key molecules released from 3D spheroids and changes in their levels in the presence of lenalidomide.

Angiopoietin-I (ANG-I), a key vascular growth factor, was detectable in all microfluidic spheroid cultures. Treatment with lenalidomide reduced ANG-1 secretion. CD137 (also referred to as Tumor Necrosis Family Receptor Superfamily member 9) and CD40 (also a member of the TNFR superfamily) were secreted, although these molecules are surface proteins. Lenalidomide decreased the amount of both these molecules. Likewise, lenalidomide treatment resulted in the downregulation of proinflammatory cytokines and chemokines such as IL-6, IL-8, CCL2 and CCL3 (Fig. 7A). IL-6 was detected in all on-chip spheroid models but reduced by lenalidomide in experimental conditions containing activated PBMCs by 2-fold.

IL8 is known to be predominantly secreted by tumor cells, macrophages and epithelial cells [40]. IL-8 was released in larger quantities by ACT-NHL spheroids compared to mono-culture spheroids, and there was a 30-fold decrease in IL8 concentration from ACT-NHL spheroids due to lenalidomide treatment (Fig. 7B). Galectin-9 (Gal-9) concentration was reduced one-fold in lenalidomide treated conditions of ACT-NHL as compared with control. In contrast, Granzyme B secretion was upregulated due to lenalidomide treatment in spheroids containing activated PBMCs, either singly (two-fold increase in protein concentration) or in co-culture NHL spheroids (20-fold increase in concentration) (Fig. 7B). Also, the release of granzyme B in the activated NHL was relatively higher at 24 h compared to 72 h since the release of granzyme B from NK cells is a rapid process [41]. Thus, secretory analysis of microfluidic spheroids clearly indicated differences in cell secretions due to immunomodulation by lenalidomide.

4. Discussion

In this study, we developed a novel microfluidics-based approach to evaluate the impact of stromal and immune cells on NHL cell survival in the course of immunomodulatory drug treatment. Few microfluidic studies have attempted to replicate the spatial organization, that is, the spherical structure observed in most carcinomas and lymphoma. Recently, some studies developed microscale models of breast and prostate cancer spheroids [42,43]. The spheroidal structure is key to regulating essential cell functions as well as responses to immunotherapeutic drug application, as shown in a conventional 3D lymphoma spheroid model [14]. To address this limitation, we developed an array of lymphoma spheroids in a droplet microfluidic platform that not only allowed us to generate multiple spheroids per experiment but also track cell growth in any given scaffold over time. Thus, the throughput of tumor construct generation is higher in droplet microfluidic platform than that obtained in microchannels. This approach is reproducible and presents an economical alternative to expensive animal models for drug screening and drug delivery studies. To tailor this approach to studying NHL drug response, we generated spheroids with a heterogeneous mixture of cells similar to the TME in NHL, that is, 75% of immune cells to 25% of non-immune cells. Immune cells such as T cells, dendritic cells and monocytes/macrophages form the largest subtype of cells in the lymphoma TME. 50% of the immune cells are composed of effector lymphocytes such as T cells [32,33]. Here, we used PBMCs since a large fraction (> 50–60%) of activated PBMCs is composed of T cells. The bone marrow fibroblast line HS-5 used here has been employed previously to generate lymphoma co-culture models [34].

An additional element in the microfluidic spheroids was the inclusion of hydrogels as 3D matrices. Naturally occurring hydrogels, such as collagen, fibrin, fibronectin and laminin have been used to evaluate cell-ECM interaction in vitro [12,13]. Type I collagen has been commonly utilized in microfluidic channels [21,22]. Alginate has long been used for tissue engineering applications and regenerative medicine due to minimal toxicity, low cost and mild cross-linking conditions (addition of cations such as Ca^{2+}). Due to the lack of cell attachment and proliferation in alginate matrices, we tested a mixture of hydrogels, alginate and puramatrix, in microfluidic spheroids for the first time [19,24–26]. Puramatrix is a 16-amino acid (Ac-[RADA]4-CONH2)) long synthetic peptide that undergoes self-assembly into β-sheets upon addition of physiological levels (in the order of millimoles) of cation solutions [23]. It is known to promote cell attachment and migration. It consists of repeats of arginine-alanine-aspartic acid-alanine (RADA) sequence and promotes cell attachment at concentrations as low as 0.1% in the scaffold. Puramatrix is currently being utilized in a number of clinical trials for cartilage, liver and neural tissue regeneration. It was used to assess the growth of another hematological cancer, multiple myeloma, but has not been used to develop lymphoma models [44]. In our study, puramatrix could not be used as a standalone material in the microfluidic perfusion system because of its low mechanical strength. The increase in elastic response of the puramatrix-mixed hydrogels in our rheological characterization suggests that cells embedded in the combination hydrogels will experience decreased resistance to motility, migration and proliferation. The addition of puramatrix also promoted the formation of hydrogels likely due to the presence of ionic self-complementary peptides which results in self-assembly [23]. Previous reports have shown the storage and loss moduli of puramatrix were lower compared to other polymers used for cell culture, although cell adhesion and proliferation were improved [23]. In future studies, further characterization by analytical techniques such as Fourier transform infrared spectroscopy (FTIR) may provide more details about the hybrid hydrogels [63].

Our study showed that addition of diluted puramatrix to alginate matrices promoted lymphoma cell aggregation and proliferation, which was significantly higher than growth in a 2D monolayer culture. The growth kinetics of cells in 2D and 3D culture conditions are distinctly different; for e.g., lymphoma cells grown in a polystyrene 3D scaffold showed greater proliferation than 2D cultures [45]. Similarly,

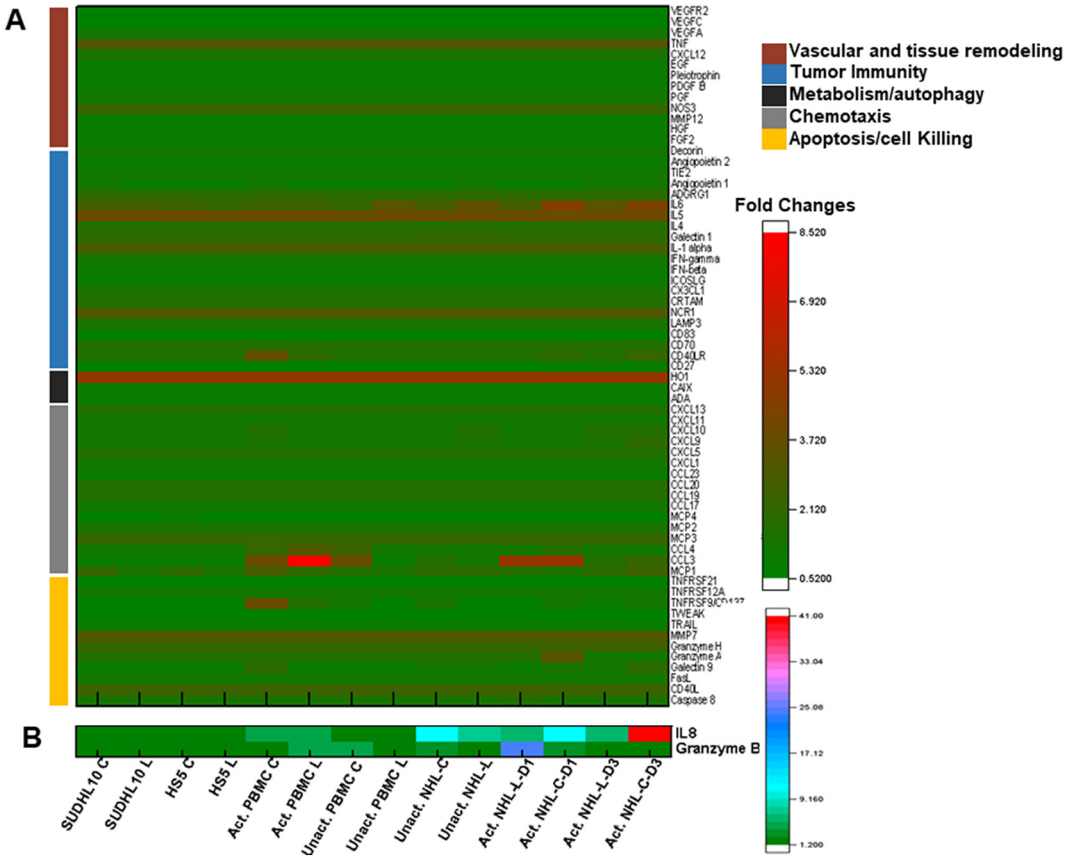

Fig. 7. Secretion profiling of perfused media collected from MF spheroid array for different experimental conditions. The concentration of secreted factors was presented as Normalized Protein eXpression (NPX). Abbreviations: C: control; L: Lenalidomide; act: activated cells; unact: non-activated cells; NHL: NHL spheroid containing all three cell types (SUDHL10, HS5 and PBMC); D1, D3: perfused media collected on Day 1 and 3 respectively. For spheroids containing single cell types, perfused media was assessed on Day 5.

fibroblasts grown in 3D released greater levels of signaling molecules compared to 2D cultures [46]. Our findings are in line with these results. Both cell proliferation and death was notably higher in 2D culture compared to 3D spheroids. We have previously observed similar responses by breast cancer cells in alginate spheroids [20]. Cancer cell death, irrespective of resistance to the chemotherapeutic drug doxorubicin, was increased in 2D monolayers in comparison with microfluidic constructs. This effect appears to be unrelated to cell type; however, further investigation is required to determine whether this holds true for other cancer subtypes or ECM combinations. Of note, the hydrogel combination utilized here did not pose a barrier to the diffusion of the small molecule drug lenalidomide, as demonstrated by differential cell response to lenalidomide in the immunogenic NHL spheroids.

Lenalidomide acts as an anti-cancer therapeutic by inducing proliferation and activation of T cells and NK cells [27, 36,37,47]. It also decreases production of pro-inflammatory cytokines but stimulates release of anti-inflammatory cytokines such as IL-2 and IFN-γ. Lenalidomide exhibits a direct anti-proliferative effect on activated B-cell like DLBCL [36,47]. The effect of lenalidomide appears to be specific to cell of origin. As expected, PBMC proliferation was increased by lenalidomide in microfluidic spheroids, whereas proliferation of SUDHL10 or HS5 cells was largely unaltered. Growth of SUDHL10 cells was significantly reduced by lenalidomide in the presence of activated PBMCs and overall cell death in the ACT-NHL was higher in lenalidomide treatment conditions as compared to control in 3D microfluidic spheroids. In future studies, these spheroids may be used to analyze the effect of novel immunomodulatory drugs and drug combinations on specific subsets of immune cells, such as T cells and NK cells, in the context of lymphoma.

In addition to cell proliferation and cytotoxicity assessment, we monitored the release of cell-secreted factors from the microfluidic spheroid arrays, which are continuously perfused. Cytokines and chemokines play a critical role in the TME. Proinflammatory cytokines promote lymphoma survival, progression and development of drug resistance. However, measuring intracellular mRNA or protein level to evaluate cytokine presence does not inform us of the levels of secreted cytokines. Previous studies have reported that monitoring secreted factors in culture media in vitro provides more insights into diseases states and helps improve the selection of therapeutic regimens [48]. Here, we collected the spheroid-perfused media and determined the presence of cytokines, chemokines, cell surface markers and cytolytic molecules. IL-6 and IL-8 have been shown to be elevated in the serum of DLBCL patients and implies poor prognosis [49–51]. Lenalidomide inhibits IL-6 secretion from activated T cells and macrophages in some cancers [52]. IL-6 was reduced post-lenalidomide treatment in immunogenic spheroids containing activated PBMCs. IL-8, secreted predominantly by tumor cells, was also decreased by lenalidomide. CCL2, a proinflammatory chemokine, is known to elevated in serum of lymphoma patients, although its exact effect in DLBCL is yet to be established [53]. CCL2, CCL3 and CCL4 were all decreased following lenalidomide treatment. Although CD137 and CD40 are surface-bound molecules, both were detected in secretions from immune cell spheroids. We hypothesize that these receptors were shed by the immune cell component of the spheroids. Studies show that CD137 and CD40 are primarily increased in CD8+ T cells and antigen presenting cells respectively [4,54,55]. Lenalidomide reduced CD137 levels compared to untreated spheroids. It has been shown previously that soluble CD137 is

released following leukocyte activation, and the shedding of this receptor may be a direct mechanism to control inflammatory responses [56,57]. It is possible that lenalidomide treatment diminishes CD137 shedding from the cell surface to promote CD137-mediated anti-tumorigenic activity. Gal-9, a negative immunomodulatory protein, is upregulated in CD4+ and CD8+ T cells in DLBCL [58]. Here, we detected Gal-9 in secretion of all immunogenic spheroids, which was decreased in the presence of lenalidomide.

Surprisingly, we detected ANG-1, a key factor associated with highly vascular TMEs, in all spheroids [59]. Lenalidomide reduced ANG-1, which has been previously shown to occur due to inhibition of Akt phosphorylation in multiple myeloma [60]. Further investigation of its mechanism in DLBCL is underway. Lastly, we detected upregulation of Granzyme B in the absence of lenalidomide in activated PBMC-containing spheroids. Granzyme B is constitutively secreted by NK cells and induces apoptosis in the target cells [61]. Lenalidomide is known to enhance the proliferation of NK cells in hematological cancers [62]. In our studies, granzyme B increased upon treatment with lenalidomide in activated immune cell spheroids. Additionally, the release of granzyme B in the activated NHL spheroids was relatively higher at 24 h compared to 72 h. This finding is in accordance with the fact that the release of granzyme B from NK cells is a relatively fast process [41]. Thus, the analysis of perfusion media from the spheroids on-chip provided an overview of key secretory molecules, but a more in-depth profiling of the dynamic changes in the secretions is required to understand their relevance in the context of DLBCL.

5. Conclusion

In summary, we report the development of a novel microfluidics-based spheroid “on-chip” approach for generation and assessment of immunogenic tumor spheroids. The complex, immune-rich TME of the spheroids can be used to assess cell proliferation, interaction and drug cytotoxicity. Our findings substantiate the effect of lenalidomide, which enhanced the proliferation and survival of the activated PBMCs, in the microfluidic platform. The spheroid array also permitted the collection and analysis of cell-secreted factors as an additional marker for detecting paracrine cell signaling in the TME. Thus, our system provides dynamic multiparametric analysis of cellular interaction and effectively recapitulates the complexities of an avascular TME. Although we generated lymphoma spheroids in this study, this approach can be used to form tumor spheroids of any type as well with other immunotherapeutic agents that may be studied. This platform should also be studied to generate patient-specific in vitro tumor models for screening and validating the optimum patient-specific immunotherapeutic strategy.

Acknowledgements

This study was partially supported by the National Institutes of Health (1R33CA223908-01).

Appendix A. Supplementary data

Supplementary data to this article can be found online at https://doi.org/10.1016/j.jconrel.2018.12.010.

References

[1] J.O. Armitage, Blood 89 (1997) 3909–3918.
[2] M. Pizzi, M. Boi, F. Bertoni, G. Inghirami, Leukemia 30 (2016) 1805.
[3] A.J. Gentles, A.M. Newman, C.L. Liu, S.V. Bratman, W. Feng, D. Kim, V.S. Nair, Y. Xu, A. Khuong, C.D. Hoang, Nat. Med. 21 (2015) 938–945.
[4] A.A. Alizadeh, A.J. Gentles, A.J. Alencar, C.L. Liu, H.E. Kohrt, R. Houot, M.J. Goldstein, S. Zhao, Y. Natkunam, R.H. Advani, Blood 118 (2011) 1350–1358.
[5] R. Küppers, Nat. Rev. Cancer 5 (2005) 251–262.
[6] J.A. Burger, P. Ghia, A. Rosenwald, F. Caligaris-Cappio, Blood 114 (2009) 3367–3375.
[7] S. Donnou, C. Galand, V. Touitou, C. Sautès-Fridman, Z. Fabry, S. Fisson, Adv. Hematol. 2012 (2012).
[8] C.-P. Day, G. Merlino, T. Van Dyke, Cell 163 (2015) 39–53.
[9] G. Yang, Q. Zhang, Y. Kong, B. Xie, M. Gao, Y. Tao, H. Xu, F. Zhan, B. Dai, J. Shi, Acta Biochim. Biophys. Sin. 47 (2015) 925–931.
[10] Y. Chu, J. Hochberg, A. Yahr, J. Ayello, C. van de Ven, M. Barth, M. Czuczman, M.S. Cairo, Cancer Immunol. Res. 3 (2015) 333–344.
[11] L.C. Cerchietti, A.F. Ghetu, X. Zhu, G.F. Da Silva, S. Zhong, M. Matthews, K.L. Bunting, J.M. Polo, C. Farès, C.H. Arrowsmith, Cancer Cell 17 (2010) 400–411.
[12] E.L. Fong, D.A. Harrington, M.C. Farach-Carson, H. Yu, Biomaterials 108 (2016) 197–213.
[13] M.E. Katt, A.L. Placone, A.D. Wong, Z.S. Xu, P.C. Searson, Front. Bioeng. Biotechnol. 4 (2016) 12.
[14] E. Decaup, C. Jean, C. Laurent, P. Gravelle, S. Fruchon, F. Capilla, A. Marrot, T. Al Saati, F. Frenois, G. Laurent, Blood Cancer J. (3) (2013) e131.
[15] K.E. Sung, D.J. Beebe, Adv. Drug Deliv. Rev. 79 (2014) 68–78.
[16] K. Kwapiszewska, A. Michalczuk, M. Rybka, R. Kwapiszewski, Z. Brzózka, Lab Chip 14 (2014) 2096–2104.
[17] B. Patra, C.-C. Peng, W.-H. Liao, C.-H. Lee, Y.-C. Tung, Sci. Rep. 6 (2016) 21061.
[18] L.J.Y. Ong, A.B. Islam, R. Dasgupta, N.G. Iyer, H.L. Leo, Y.-C. Toh, Biofabrication 9 (2017) 045005.
[19] S.-Y. Jeong, J.-H. Lee, Y. Shin, S. Chung, H.-J. Kuh, PLoS ONE 11 (2016) e0159013.
[20] P. Sabhachandani, V. Motwani, N. Cohen, S. Sarkar, V. Torchilin, T. Konry, Lab Chip 16 (2016) 497–505.
[21] I.K. Zervantonakis, S.K. Hughes-Alford, J.L. Charest, J.S. Condeelis, F.B. Gertler, R.D. Kamm, Proc. Natl. Acad. Sci. U. S. A. 109 (2012) 13515–13520.
[22] S. Parlato, A. De Ninno, R. Molfetta, E. Toschi, D. Salerno, A. Mencattini, G. Romagnoli, A. Fragale, L. Roccazzello, M. Buoncervello, Sci. Rep. 7 (2017) 1093.
[23] N. Akiyama, T. Yamamoto-Fukuda, H. Takahashi, T. Koji, Int. J. Nanomedicine 8 (2013) 2629.
[24] C.-C. Wang, K.-C. Yang, K.-H. Lin, H.-C. Liu, F.-H. Lin, Biomaterials 32 (2011) 7118–7126.
[25] A.D. Augst, H.J. Kong, D.J. Mooney, Macromol. Biosci. 6 (2006) 623–633.
[26] M.W. Tibbitt, K.S. Anseth, Biotechnol. Bioeng. 103 (2009) 655–663.
[27] P.H. Wiernik, I.S. Lossos, J.M. Tuscano, G. Justice, J.M. Vose, C.E. Cole, W. Lam, K. McBride, K. Wride, D. Pietronigro, J. Clin. Oncol. 26 (2008) 4952–4957.
[28] C.B. da Cunha, D.D. Klumpers, W.A. Li, S.T. Koshy, J.C. Weaver, O. Chaudhuri, P.L. Granja, D.J. Mooney, Biomaterials 35 (2014) 8927–8936.
[29] Y. Xu, X. Wang, Biotechnol. Bioeng. 112 (2015) 1683–1695.
[30] T. Andersen, P. Auk-Emblem, M. Dornish, Microarrays 4 (2015) 133–161.
[31] F. Yuan, M. Dellian, D. Fukumura, M. Leunig, D.A. Berk, V.P. Torchilin, R.K. Jain, Cancer Res. 55 (1995) 3752–3756.
[32] Z.-Z. Yang, S.M. Ansell, Clin. Adv. Hematol. Oncol. 10 (2012) 810–818.
[33] B. Herreros, A. Sanchez-Aguilera, M. Piris, Leukemia 22 (2008) 49.
[34] M. Rahmani, M.M. Aust, E.C. Benson, L. Wallace, J. Friedberg, S. Grant, Clin. Cancer Res. 20 (2014) 4849–4860.
[35] L. Yu, M.C. Chen, K.C. Cheung, Lab Chip 10 (2010) 2424–2432.
[36] A. Kritharis, M. Coyle, J. Sharma, A.M. Evens, Blood 125 (2015) 2471–2476.
[37] A.A. Chanan-Khan, B.D. Cheson, J. Clin. Oncol. 26 (2008) 1544–1552.
[38] M. Dimopoulos, M. Hussein, A. Swern, D. Weber, Leukemia 2011 (25) (1620).
[39] R. Leblanc, T. Hideshima, L.P. Catley, R. Shringarpure, R. Burger, N. Mitsiades, C. Mitsiades, P. Cheema, D. Chauhan, P.G. Richardson, Blood 103 (2004) 1787–1790.
[40] D.J. Waugh, C. Wilson, Clin. Cancer Res. 14 (2008) 6735–6741.
[41] L. Wu, M. Adams, T. Carter, R. Chen, G. Muller, D. Stirling, P. Schafer, J.B. Bartlett, Clin. Cancer Res. 14 (2008) 4650–4657.
[42] B. Kwak, Y. Lee, J. Lee, S. Lee, J. Lim, J. Control. Release 275 (2018) 201–207.
[43] E.O. Mosaad, K.F. Chambers, K. Futrega, J.A. Clements, M.R. Doran, Sci. Rep. 10 (2018) 253 8(1).
[44] J. Jakubikova, D. Cholujova, T. Hideshima, P. Gronesova, A. Soltysova, T. Harada, J. Joo, S.-Y. Kong, R.E. Szalat, P.G. Richardson, Oncotarget 7 (2016) 77326.
[45] C.E. Caicedo-Carvajal, Q. Liu, Y. Remache, A. Goy, K.S. Suh, J. Tissue Eng. 2011 (2011).
[46] K.E. Sung, X. Su, E. Berthier, C. Pehlke, A. Friedl, D.J. Beebe, PLoS ONE (8) (2013) e76373.
[47] J.G. Gribben, N. Fowler, F. Morschhauser, J. Clin. Oncol. 33 (2015) 2803–2811.
[48] A. Gloghini, I. Bongarzone, Cell-Secreted Signals Shape Lymphoma Identity, Seminars in Cancer Biology, Elsevier, 2015, pp. 81–91.
[49] M. Sahebjamee, M. Eslami, F. Atarbashimoghadam, A. Sarafnejad, Med. Oral Patol. Oral Cir. Bucal. 13 (2008) 292.
[50] W. He, L. Luistro, D. Carvajal, M. Smith, T. Nevins, X. Yin, J. Cai, B. Higgins, K. Kolinsky, C. Rizzo, Mol. Oncol. 5 (2011) 292–301.
[51] A. Načinović-Duletić, S. Štifter, Š. Dvornik, Ž. Škunca, N. Jonjić, Int. J. Lab. Hematol. 30 (2008) 230–239.
[52] M. Semeraro, E. Vacchelli, A. Eggermont, J. Galon, L. Zitvogel, G. Kroemer, L. Galluzzi, OncoImmunology 2 (2013) e26494.
[53] G. Mazur, I. Kryczek, T. Wrobel, D. Dlubek, A. Klimczak, E. Jaskula, M. Jelen, A. Lange, K. Kuliczkowski, Folia Histochem. Cytobiol. 49 (2006) 240–247.
[54] V.Y. Taraban, T.F. Rowley, L. O'Brien, H. Chan, L.E. Haswell, M.H. Green, A.L. Tutt, M.J. Glennie, A. Al-Shamkhani, Eur. J. Immunol. 32 (2002) 3617–3627.
[55] A. Chatzigeorgiou, M. Lyberi, G. Chatzilymperis, A. Nezos, E. Kamper, Biofactors 35 (2009) 474–483.
[56] J. Michel, J. Langstein, F. Hofstädter, H. Schwarz, Eur. J. Immunol. 28 (1998) 290–295.
[57] G.M. McGeehan, J.D. Becherer, R.C. Bast Jr., C.M. Boyer, B. Champion,

K.M. Connolly, J.G. Conway, P. Furdon, S. Karp, S. Kidao, Nature 370 (1994) 558–561.
[58] L. Zhang, H. Du, T.-W. Xiao, J.-Z. Liu, G.-Z. Liu, J.-X. Wang, G.-Y. Li, L.-X. Wang, Biomed. Pharmacother. 75 (2015) 83–87.
[59] H. Huang, A. Bhat, G. Woodnutt, R. Lappe, Nat. Rev. Cancer 10 (2010) 575.
[60] K. Dredge, R. Horsfall, S.P. Robinson, L.-H. Zhang, L. Lu, Y. Tang, M.A. Shirley, G. Muller, P. Schafer, D. Stirling, Microvasc. Res. 69 (2005) 56–63.
[61] M.D. Prakash, C.H. Bird, P.I. Bird, Immunol. Cell Biol. 87 (2009) 249.
[62] B.M.B. Souza, F.B. De Vito, M.L. Calado, M.V. Silva, L.R. Oliveira, V. Rodrigues-Júnior, H. Moraes-Souza, Leuk. Lymphoma 59 (2018) 214–220.
[63] D.P. Suhas, A.V. Raghu, H.M. Jeong, T.M. Aminabhavi, RSC Adv. 3 (2013) 17120–17130.